JOURNAL OF MOLECULAR RECOGNITION
J. Mol. Recognit. 2007; **20**: 215–226
Published online in Wiley InterScience
(www.interscience.wiley.com) DOI:10.1002/jmr.840

Docking study and free energy simulation of the complex between p53 DNA-binding domain and azurin

Valentina De Grandis, Anna Rita Bizzarri* and Salvatore Cannistraro

Biophysics and Nanoscience Centre, CNISM, Facoltà di Scienze, Università della Tuscia, Largo dell'Università—I-01100 Viterbo, Italy

Molecular interaction between p53 tumor suppressor and the copper protein azurin (AZ) has been demonstrated to enhance p53 stability and hence antitumoral function, opening new perspectives in cancer treatment. While some experimental work has provided evidence for AZ binding to p53, no crystal structure for the p53–AZ complex was solved thus far. In this work the association between AZ and the p53 DNA-binding domain (DBD) was investigated by computational methods. Using a combination of rigid-body protein docking, experimental mutagenesis information, and cluster analysis 10 main p53 DBD–AZ binding modes were generated. The resulting structures were further characterized by molecular dynamics (MD) simulations and free energy calculations. We found that the highest scored docking conformation for the p53 DBD–AZ complex also yielded the most favorable free energy value. This best three-dimensional model for the complex was validated by using a computational mutagenesis strategy. In this structure AZ binds to the flexible L_1 and s_7–s_8 loops of the p53 DBD and stabilizes them through protein–protein tight packing interactions, resulting in high degree of both surface matching and electrostatic complementarity.

Keywords: **p53; azurin; docking; molecular dynamics simulation; free energy**

Received 12 June 2007; revised 4 July 2007; accepted 10 July 2007

INTRODUCTION

p53 tumor suppressor is a complex multifunctional protein that acts as a 'guardian of the genome' in preventing cancer growth and maintaining genomic stability (Vogelstein *et al*., 2000). In response to DNA damage and cellular oncogenic stress, p53 exerts its antitumoral activity by regulating the transcription of numerous genes involved in cell cycle control and apoptosis. Mutations in the p53 protein are the most frequent genetic alterations in human cancer (Veprintsev *et al*., 2006). Over half of all cancers carry p53 mutations disrupting their normal biological function and many other tumorigenic mutations result in altered p53 structure and stability (Wong *et al*., 1999; Joerger *et al*., 2006). The search for molecules able to restore transcriptional activity to mutant p53 or stabilize the wild-type (WT) protein represents therefore a key issue to make progress in cancer treatment therapies.

Yamada *et al*. (2004) have recently demonstrated that the blue copper protein azurin (AZ) from *Pseudomonas aeruginosa* can enter human cancer cells and form a complex with p53, stabilizing it and enhancing its intracellular levels, thereby activating apoptosis and growth arrest in such cells. When injected in nude mice harboring human melanoma (Yamada *et al*., 2002) or breast cancer (Punj *et al*., 2004) cells, AZ induces tumor regression but, in contrast with live bacteria previously tested against cancers, shows no toxicity or harmful side effects. These results make AZ an attractive candidate for developing novel anticancer strategies (Yamada *et al*., 2002, 2004; Punji *et al*., 2003; Punj *et al*., 2004; Apiyo and Wittung-Stafshede, 2005).

Although some previous experimental work has demonstrated AZ binding to p53, the molecular mechanisms underlying p53–AZ complex formation are not yet well understood. To gain further insight about p53–AZ binding mode it is necessary to deeply characterize the interface between the two proteins, investigating on specific domains of AZ and p53 involved in their association.

AZ is a 128-residues β-barrel protein which acts as an electron-transfer shuttle in the respiratory chain of denitrifying bacteria. Its structure, dynamics, and functionality as well as its interactions with redox partners have been well characterized by both experimental techniques (Nar *et al*., 1991; Webb and Loppnow, 1999; Bonanni *et al*., 2005) and computational methods (Arcangeli *et al*., 1999; De Rienzo *et al*., 2000; Bizzarri, 2006; Cascella *et al*., 2006; Bizzarri *et al*., 2007).

p53 consists of four identical 393-residues chains, each chain being comprised of four functional regions: an N-terminal domain (NTD), containing an acidic transcriptional activation domain and a proline-rich domain, a sequence-specific DNA-binding domain (DBD), a tetramerization domain (TD), and a C-terminal regulatory domain (CTD) (Bell *et al*., 2002; Veprintsev *et al*., 2006).

*Correspondence to: A. R. Bizzarri, Biophysics and Nanoscience Centre, CNISM, Facoltà di Scienze, Università della Tuscia, Largo dell'Università—I-01100 Viterbo, Italy. E-mail: bizzarri@unitus.it

The DBD is the largest p53 domain and contains the binding sites for interaction with DNA. This domain was found to have a relatively unstable structure and it is susceptible to many tumorigenic mutations, inactivating it by either lowering its stability or altering its native conformation (Joerger *et al*., 2006; Liu *et al*., 2006; Pérez Cañadillas *et al*., 2006). The p53 DBD and TD structures have been well characterized both by nuclear magnetic resonance (NMR) and X-ray crystallography (Cho *et al*., 1994; Clore *et al*., 1994; Jeffrey *et al*., 1995; Klein *et al*., 2001). While the DBD and TD form globular well-folded domains, the p53 N- and C-terminal regions are mostly unstructured under physiological conditions (Dawson *et al*., 2003; Weinberg *et al*., 2004). The presence of these unfolded regions is probably the reason for which the crystal structure for the full-length p53 protein has not yet been defined. The large size of the p53 tetramer is also at the limit of standard NMR techniques (Veprintsev *et al*., 2006).

Regarding the p53–AZ complex, the molecular interaction between the two proteins has been the subject of different experimental studies. Glycerol gradient ultracentrifugation followed by pull-down assays and calorimetric experiments were performed to examine p53–AZ complex formation as well as to investigate the interaction domains of these two proteins (Yamada *et al*., 2002; Masatoshi *et al*., 2003; Punji *et al*., 2003; Punj *et al*., 2004; Yamada *et al*., 2004; Apiyo and Wittung-Stafshede, 2005). The results of these studies suggest that AZ binds to the p53 DBD and perhaps also to the NTD, while the p53 CTD is defective in complex formation with AZ (Punji *et al*., 2003; Apiyo and Wittung-Stafshede, 2005). Site-directed mutagenesis strategies have been also applied to map individual residues in AZ binding interface. Both apo-AZ devoid of copper and redox-negative AZ mutants such as Cys112Asp (C112D) and Met44LysMet64Glu (M44KM64E) were investigated for complex formation with p53 and compared with the WT protein. While apo-AZ and the C112D mutant were found to form stable complexes with p53, the M44KM64E mutant was demonstrated to be defective in complex formation with p53 (Yamada *et al*., 2002; Yamada *et al*., 2004), indicating, therefore, that AZ hydrophobic patch (HP) surrounding residues Met 44 and Met 64, important for AZ interactions with redox partners, is also involved in p53 binding. Moreover the specificity and the biorecognition between AZ and p53 was investigated by recent atomic force spectroscopy experiments, that allowed evaluating the protein–protein interaction forces and the complex dissociation rate (Taranta M, Bizzarri AR, Cannistraro S, unpublished).

However, since no molecular structure for this complex has been determined, most likely due to the same experimental difficulties as those involved in solving the p53 structure, its real spatial arrangement is still missing. In this respect, more structural information—for example, which specific residues make up the binding sites of the two proteins—is crucially important to make progress in understanding the nature of p53–AZ interaction.

One of the most promising approaches for modeling molecular interactions is protein docking, which aims to predict the structure of a protein–protein complex starting from the independently solved structures of the components (Vajda and Camacho, 2004). Docking methods may be coupled with refinement and re-ranking techniques, including algorithms for energy minimization, molecular dynamics (MD) simulations, and schemes for filtering and clustering of resulting predictions, to discriminate near-native docked conformations from false positive hits, improving thus the quality of the obtained solutions (Halperin *et al*., 2002).

In this work a computational strategy combining protein docking with experimental mutagenesis information, cluster analysis, and MD binding free energy simulations was employed to investigate the interaction between AZ and the p53 DBD. We have used the Zdock docking program which combines pairwise shape complementarity with desolvation and electrostatics (Chen and Weng, 2002; Chen and Weng, 2003). Such a program is particularly suitable to investigate our system in which the presence of charged residues at the interface of the protein partners might have some relevance in the complex formation. A molecular model for the p53 DBD–AZ complex was built, in which extensive hydrogen-bonding and packing interactions are established between the HP of AZ and the highly flexible p53 DBD peripheral loops. The reliability for the resulting model was evaluated by performing computational mutagenesis on AZ key residues (Met 44 and Met 64) known to interact with p53. The predicted complex provides a structural basis for understanding p53–AZ interaction and reveals a possible molecular explanation for the p53-stabilizing ability of AZ.

METHODS

Molecular systems

Initial atomic coordinates of AZ were taken from the X-ray structure at 1.93 Å resolution (chain B of PDB entry 4AZU) (Nar *et al*., 1991). The protein, shown on the left in Figure 1, consists of an α-helix (H) and eight β-strands (β_1–β_8) that form two sheets arranged in a Greek key motif. The copper ion, located at the northern end of the molecule about 7 Å below the surface, is coordinated by three strong equatorial ligands (N^{δ} of His 46 and His 117 and S^{γ} of Cys 112) and two weaker axial ligands (S^{δ} of Met 121 and the backbone oxygen of Gly 45). The copper ligand His 117 is surrounded by a cluster of hydrophobic residues, known as the HP. A disulfide bridge connecting residues Cys 3 and Cys 26 in the southern region of the protein contributes to the high stability of AZ (Bonander *et al.,* 2000).

The initial p53 DBD configuration (shown on the right in Figure 1) was taken from chain B of PDB entry 1TUP, describing the 2.2 Å resolution crystal structure of this domain in complex with a consensus DNA-binding site (Cho *et al*., 1994). The p53 DBD consists of a β-sandwich formed by two antiparallel β-sheets, S_I and S_{II}, containing four (s_1, s_3, s_5, and s_8) and five (s_4, s_6, s_7, s_9, and the N-termini of s_{10}) strands, respectively. The β-sandwich structure acts as a scaffold for two large loops, L_2 and L_3, and a loop–sheet–helix motif (L_1–S_{III}–H_2). L_1 is connected to the H_2 α-helix by the three-stranded S_{III} sheet, containing the s_2–s_2' β-hairpin and the C-termini of s_{10}. L_2 contains the short H_1 helix connecting strands s_4–s_5 while L_3 occurs between strands s_8 and s_9. DNA is bound by L_1 and L_3—the H_2 helix and L_1 loop fit into the major groove and L_3 binds to the minor groove. The L_2 loop acts to stabilize

DOI: 10.1002/jmr

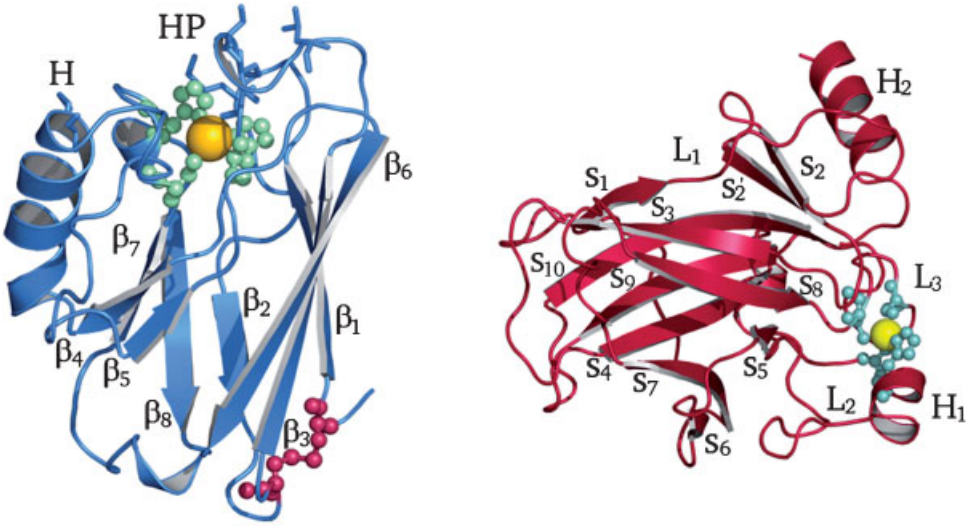

Figure 1. Three-dimensional structures of AZ (on the left) and p53 DBD (on the right). The active site of AZ and the zinc-finger of the p53 DBD are shown as ball and stick models. The HP of AZ is depicted in licorice representation and the Cys 3–Cys 26 disulfide bridge is shown in magenta.

the L_3 loop by packing against it. Loops L_2 and L_3 are connected by a zinc ion, which is tetrahedrally coordinated by the side-chains of residues Cys 176, His 179, Cys 238, and Cys 242, forming a Cys_3His zinc-finger motif (Duan and Nilsson, 2006).

Protein docking

Our docking simulation consists of two steps. In the initial stage we employed the Zdock method to generate a set of possible configurations for the p53 DBD–AZ complex. Zdock (Chen and Weng, 2002) is a rigid-body docking algorithm using a Fast Fourier Transform (FFT) to perform an exhaustive six-dimensional search in the translational and rotational space between the two molecules. Each protein is projected into a three-dimensional grid and different values are assigned to the cells of the grid, representing the surface or the interior of the molecules. Zdock searches orientational space by rotating the ligand around its geometric center with the receptor protein kept fixed in space. For each sampled angle only the ligand translation corresponding to the best geometric match between the two proteins is retained. The obtained configurations for the complex are ranked based on a scoring function combining shape complementarity, desolvation energy, and electrostatics. The metal ions belonging to the protein structures (copper AZ and zinc in p53) were included during the docking.

In our simulation the p53 DBD was kept fixed whereas AZ was allowed to rotate and translate in order to explore the conformational space for the complex. Docking samplings were carried out by employing a $128 \times 128 \times 128$ point grid with a spacing of 1.2 Å and a rotational interval of 6°.

The top 2000 complexes predicted by Zdock were filtered to select binding modes consistent with the available experimental mutagenesis data. For this purpose we applied a distance constraint between the p53 DBD–AZ interface residues. Only those models in which both the AZ residues Met 44 and Met 64 are within a distance cut-off of 6 Å from the p53 DBD were considered further. The filtering process reduced the number of candidate models to 194.

In the second stage of our docking study the obtained structures were grouped in clusters to eliminate very similar conformations. For this purpose, we used the ClusPro docking server, which performs cluster analysis by means of a pairwise binding site root mean squared deviation (RMSD) criterion. Details on the ClusPro algorithm can be found in Comeau *et al*. (2004). The clustering radius was set to $R_c = 6$ Å. The top 20 clusters generated by ClusPro were retained for further analysis.

MD simulations

MD simulations were performed with the GROMACS 3.2.1 package, using the GROMOS96 43a1 forcefield (van der Spoel *et al*., 2001). Each complex was solvated in a simple point charge (SPC) water box (Berendsen *et al*., 1969) extending to at least 6 Å from the complex surface.

AZ active site was modeled by applying bond-stretching and bond-bending harmonic potentials between the copper ion and the nitrogen atoms of His 46 and His 117 and the sulfur atom of Cys 112, while the interactions of copper with the thioether sulfur of Met 121 and the carbonyl oxygen of Gly 45 were treated by a non-bonded approach (Arcangeli *et al*., 1999; Bizzarri, 2006; Bizzarri *et al*., 2007). The partial charges describing AZ active site were assigned according to Swart (2002). Only the Cu charge was modified with respect to Swart (2002) to ensure an integer charge value for AZ: $q_{Cu} = 0.686e$, giving a net AZ charge of $-2.000e$.

The zinc-finger topology in the p53 DBD was described through a bonded approach, according to Calimet and Simonson (2006). Zinc was bound to four ligands: three sulfures from Cys 176, Cys 238, and Cys 242 and one nitrogen from His 179. The zinc charge was fixed to $1.000e$. The covalent character of Zn–S bonds was taken into

DOI: 10.1002/jmr

account by modeling the Zn-Cys charge transfer as in Maynard and Covell (2001). The value for the p53 DBD electric charge resulted 3.000*e*.

A chloride counterion was added to the simulation box to keep the simulated systems neutral. The MD simulations were carried out in the NPT ensemble with $T = 300$ K and $P = 1$ bar. The Nose–Hoover thermostat method was used to control the system temperature, with coupling time constant $\tau_T = 0.1$ ps. Constant pressure was imposed using the Parrinello–Rahman extended-ensemble ($\tau_P = 1.0$ ps). The long-range electrostatics were treated with the Particle Mesh Ewald (PME) method with a lattice spacing of 1.2 Å. A 9 Å cut-off was employed for Lennard–Jones interactions. The pair list was updated every 10 MD steps. All covalent bonds were constrained with the LINCS algorithm (Hess *et al*., 1997). The time step was chosen to be 2 fs. The complexes were minimized with steepest descent and gradually heated from 50 to 300 K at 20 ps increments of 50 K. The systems were then equilibrated by a 600 ps MD simulation under position restraints. Finally an unrestrained MD run was carried out for 3 ns. The first 1.5 ns of the run was treated as a further equilibration simulation and the remainder 1.5 ns was for data collection. Snapshots of the complexes were recorded every 10 ps for later binding free energy analysis.

Calculation of the binding free energy

The p53 DBD–AZ interaction free energies were evaluated with the Molecular Mechanics Poisson-Boltzmann Surface Area (MM-PBSA) method (Srinivasan *et al*., 1998). This procedure is based on a combination of MM and continuum solvent approaches to give an estimation for the binding free energy of a protein complex: $G_{\text{binding}} = G_{\text{complex}} - G_{\text{receptor}} - G_{\text{ligand}}$, where the free energy of each term can be calculated as:

$$G = E_{\text{MM}} - TS_{\text{MM}} + G_{\text{solv}} \quad (1)$$

In Equation (1) the free energy is splitted into a 'gas phase' term, containing internal energy (E_{MM}) and entropic (TS_{MM}) parts, and a solvation contribution (G_{solv}), the three terms being averaged over a set of snapshots for the complex, the receptor, and the ligand stored during a MD simulation. The solvation term G_{solv} can be further decomposed into electrostatic ($G_{\text{polar,solv}}$) and non-polar ($G_{\text{non-polar,solv}}$) parts (Massova and Kollman, 1999). The snapshot structures for the free energy calculations of complexes and separated proteins were taken from the MD trajectories collected for protein–protein complexes, based on the assumption, frequently made in similar studies, that no changes occur in the receptor and ligand conformations upon binding (Ganoth *et al*., 2006).

The E_{MM} energy can be written as $E_{\text{MM}} = E_{\text{elec}} + E_{\text{VdW}}$, where the two terms represent the protein–protein electrostatic and Van der Waals interaction energies, respectively.

The entropic contribution to the free energy was neglected in our simulation, based on the assumption that the TS_{MM} terms for different docking modes of the same protein complex should be similar and therefore cancel out when relative binding free energies between them are calculated (Wu *et al*., 2004).

The electrostatic part of the solvation free energy was obtained by numerically solving the Poisson–Boltzmann equation with the Adaptive Poisson–Boltzmann Solver (APBS) software (Baker *et al*., 2001). The grid-spacing was set to 0.25 Å. We used the GROMOS96 43a1 forcefield parameter set for atomic charges and radii and a probe radius of 1.4 Å to define the dielectric boundary. The interior dielectric constant for the complexes was 4 and the water dielectric constant was set to 80 (Ganoth *et al*., 2006).

The non-polar contribution to G_{solv} was taken to be proportional to the solvent accessible surface area (SASA): $G_{\text{non-polar,solv}} = \gamma \text{SASA} + \beta$, with $\gamma = 2.2\ \text{kJ mol}^{-1}\ \text{nm}^{-2}$ and $\beta = 3.84\ \text{kJ mol}^{-1}$ (Chong *et al*., 1999).

For each simulated complex all calculations were averaged over 150 snapshot structures.

Computational mutagenesis

The best p53 DBD–AZ binding mode was validated by investigating binding free energy changes upon replacement of the hydrophobic residues Met 44 and Met 64 in AZ docking interface by two polar charged residues (M44KM64E), drawing on previous experimental studies about p53–AZ complex formation. The starting structure for the p53 DBD–AZ M44KM64E complex was built from the best WT docking model by using the Swiss-Pdb Viewer (Guex and Peitsch, 1997). The mutant was relaxed by energy minimization followed by 3 ns MD simulation run to remove any steric conflicts. MD simulation and energetic analysis for the mutant complex were performed as described above for WT models.

Figure preparation

Figures were created with Pymol (http://pymol.sourceforge.net).

RESULTS AND DISCUSSION

Docking of the p53 DBD–AZ complex

The Zdock method combined with experimental mutagenesis data and the ClusPro clustering scheme allowed generating 20 candidate p53 DBD–AZ configurations. The 3D structures of these models were compared with each other by using the VMD software (Humphrey *et al*., 1996). The models whose geometrical structures were found to be similar were grouped together, based on a RMSD criterion: each group consisted of conformations differing by a maximum backbone-atoms RMSD of 7.0 Å from each other. Ten groups of configurations thus emerged. The highest ranked model in each group was retained for further analysis. The physical properties of protein–protein interfaces for the obtained models, as calculated by means of the protein–protein interaction server (PPI server) (Jones and Thornton, 1996), are listed in Table 1.

DOI: 10.1002/jmr

Table 1. Interface parameters for the 10 docking models of the p53 DBD–AZ complex

					p53 DBD		AZ	
Model	ClusPro ranking order	Group	ASA (Å^2)	HB	Percentage of polar atoms in interface	Percentage of non-polar atoms in interface	Percentage of polar atoms in interface	Percentage of non-polar atoms in interface
1	1	I	879.2	4	47.5	52.5	33.3	66.7
2	2	III	697.2	4	42.0	57.9	29.8	70.2
3	4	IV	700.7	1	33.2	66.8	31.6	68.4
4	5	IV	891.6	2	40.1	59.8	38.5	61.5
5	8	I	723.3	5	45.0	55.0	35.6	64.4
6	9	IV	739.4	5	35.9	64.1	27.1	72.9
7	11	II	869.1	2	36.9	63.0	26.8	73.2
8	14	III	849.0	4	46.3	53.7	34.0	66.0
9	16	III	773.5	3	47.0	53.0	43.1	56.9
10	20	II	821.3	4	48.9	51.1	39.7	60.3

The interface accessible surface area (ASA), defined as the difference in water accessible surface area between the protein complex and the separated proteins, provides information on the protein–protein steric fit—the bigger the ASA, the higher the shape complementarity between the two molecules. All the models have interfaces burying areas in the range 690–890 Å^2, similar to those expected for transient complexes (400–1000 Å^2) and lower than those commonly observed for permanent complexes (1000–2000 Å^2), such as enzymes and their inhibitors, with a high degree of shape complementary (Nooren and Thornton, 2003). Table 1 also reports that in all models the two proteins exhibit predominantly non-polar interfaces, responsible of short-range hydrophobic interaction stabilizing the complex (Sheinerman *et al*., 2000). The fifth column of Table 1 finally lists the number of p53 DBD–AZ hydrogen bonds (HBs) (McDonald and Thornton, 1994). In the 10 models one to five HBs are established between the two proteins, conferring specificity to p53 DBD–AZ biomolecular recognition.

To further characterize the 10 models, protein residues at the p53 DBD–AZ interface were investigated. According to the filter applied to our docking solutions, AZ interface contains its HP for all 10 models. The p53 DBD interaction domains are instead markedly different among the candidate configurations. Based on the p53 DBD docking sites, the 10 models can be, in particular, divided into four groups (I–IV), each group consisting of structures characterized by similar p53 DBD binding sites for AZ but different AZ orientations with respect to the p53 DBD.

The configurations in groups I and II (shown in panels A and B of Figure 2, respectively) are characterized by AZ binding to the L_1 loop and s_3 strand of the p53 DBD. Moreover in group I the p53 DBD docking sites also involve the s_7–s_8 loop and s_8 strand, while in group II the p53 DBD interface consists of the s_2–s_2' loop other than L_1 and s_3. Regarding group I, the major differences between models 1 and 5 are seen in AZ binding site for the p53 DBD. In model 1 AZ interface contains β_2, β_8 and the β_1–β_2, and β_3–β_4 loops, while in model 5 AZ binds to the p53 DBD through the β_3–β_4 and β_4–β_5 loops. Differences in AZ binding surface are observed also between the two models in group II. In model 7 AZ docking site is made up of the two loops bridging β_1–β_2 and β_4–β_5, whereas in model 10 AZ binds to the p53 DBD through the β_1 strand and β_3–β_4 loop. Moreover in model 7 the p53 DBD binding site also involves the protein C-termini, while in model 10 it is displaced towards the initial portion of L_1.

In the models of groups III and IV (depicted in panels A and B of Figure 3, respectively), the p53 DBD binding sites are mainly located on the L_2 and s_6–s_7 loops. In group III the p53 DBD interfacial region also comprises the s_7 strand. Regarding AZ binding surface, in model 2 it is formed by the β_1–β_2 loop and β_2 strand, while in model 8 AZ interface contains protein domains connecting strands β_3–β_4, β_4–β_5, and β_7–β_8. In model 9 AZ interaction sites are mainly located in its N-terminal region, being made up of the β_1 strand other than the HP. In group IV also the L_3 loop participates to p53 DBD–AZ interaction. In model 3 AZ binds to the p53 DBD through residues in the β_7–β_8 loop and H α-helix, while in model 4 AZ docking sites involve the β_1–β_2 and β_7–β_8 loops and β_8 strand and in model 6 AZ interface consists of the β_3–β_4 and β_4–β_5 loops along with the HP.

Concerning the ability of the p53 DBD to interact with other partners upon binding with AZ, we remark that these interactions are not necessarily mutually exclusive. Indeed, as suggested by ASA values reported in Table 1, it may be possible that the molecular complex between AZ and the p53 DBD is transient in nature and it rapidly dissociates after inducing apoptosis, achieving thus p53 DBD interaction with other proteins. Based on these considerations, binding free energy analysis was carried out on the full set of docking models, including those belonging to group IV, for deeply exploring the entire range of the possible p53 DBD–AZ binding modes.

MD simulations of the p53 DBD–AZ complex

The 10 candidate p53 DBD–AZ conformations were subjected to further refinement by MD simulations to model protein flexibility and solvation effects. Table 2 lists average values of the RMSD from the starting structure and the interface parameters for our models, evaluated over snapshots extracted at 100 ps intervals during the last 1.5 ns of the MD runs. As shown in Table 2, during the simulations

DOI: 10.1002/jmr

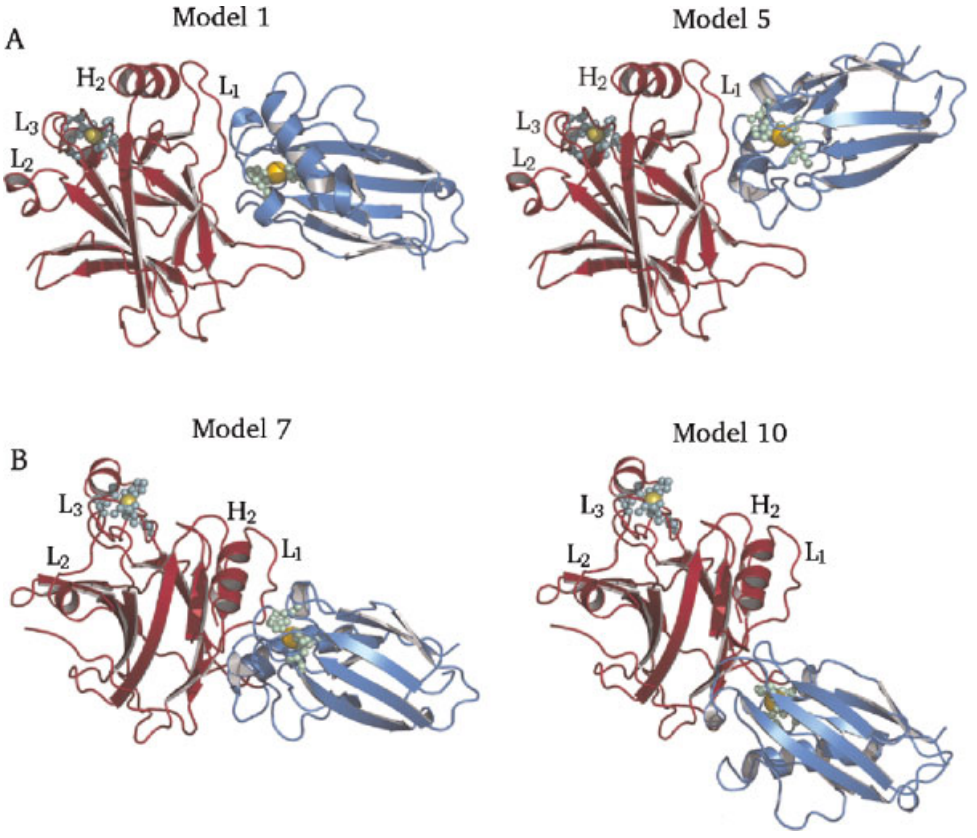

Figure 2. Three-dimensional structures of docking models in groups I and II. Models 1 (on the left) and 5 (on the right) of group I are reported in panel A. Models 7 and 10 of group II are shown from left to right in panel B. This figure is available in colour online at www.interscience.wiley.com/journal/jmr

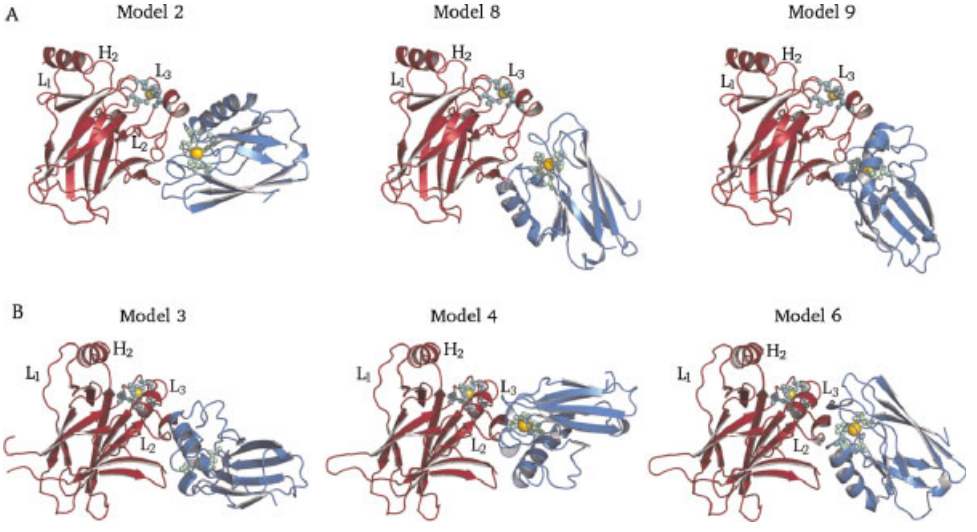

Figure 3. Three-dimensional structures of docking models in groups III and IV. Models 2, 8, and 9 of group III are reported in the left, central, and right parts of panel A, respectively. Models 3, 4, and 6 of group IV are shown from left to right in panel B. This figure is available in colour online at www.interscience.wiley.com/journal/jmr

conformational changes occurred in all 10 models, the time-averaged RMSD being in the range 2.7–4.4 Å. Interestingly, the structural evolution of p53 DBD–AZ binding interface with respect to the docking models (see Table 1) in groups I and II is markedly different with respect to groups III and IV.

The interface areas in groups I and II strongly increased during the simulations, while ASA of groups III and IV were found to decrease or remain approximately constant. The high ASA exhibited by groups I and II can be ascribed to the presence of the L_1 loop, and also the s_7–s_8 loop in the case of group I, in the p53 DBD binding interface for AZ. These

DOI: 10.1002/jmr

Table 2. RMSD and interface parameters for the 10 p53 DBD–AZ models averaged over the MD simulation runs

					p53 DBD		AZ	
Model	Group	RMSD (Å)	ASA (Å^2)	HB	Percentage of polar atoms in Interface	Percentage of non-polar atoms in interface	Percentage of polar Atoms in Interface	Percentage of non-polar atoms in interface
1	I	3.2 (0.1)	978.0 (30.3)	11.8 (2.3)	44.4 (3.0)	55.6 (3.0)	36.9 (2.3)	63.0 (2.3)
2	III	2.7 (0.2)	731.7 (40.9)	5.7 (2.1)	48.0 (3.3)	51.9 (3.3)	29.4 (3.7)	70.9 (3.7)
3	IV	3.1 (0.2)	739.8 (31.5)	3.1 (1.3)	48.6 (2.1)	51.4 (2.1)	32.8 (3.0)	67.1 (3.0)
4	IV	3.8 (0.3)	721.8 (41.0)	4.2 (1.1)	50.6 (2.5)	49.3 (2.5)	30.5 (4.3)	69.4 (4.3)
5	I	2.9 (0.1)	838.2 (37.3)	8.4 (1.1)	37.8 (3.0)	62.2 (3.0)	27.0 (3.1)	72.9 (3.1)
6	IV	2.3 (0.3)	769.0 (36.9)	5.9 (2.0)	48.4 (3.6)	51.5 (3.6)	28.5 (3.5)	71.4 (3.5)
7	II	3.0 (0.2)	1061.7 (76.9)	7.4 (0.4)	39.5 (2.4)	60.5 (2.4)	31.7 (2.3)	68.3 (2.3)
8	III	4.4 (0.2)	687.8 (44.3)	5.6 (1.7)	41.1 (3.5)	51.8 (3.5)	34.3 (2.9)	65.6 (2.9)
9	III	3.4 (0.3)	804.3 (59.5)	4.4 (2.4)	46.5 (3.6)	53.4 (3.6)	35.5 (3.3)	64.5 (3.3)
10	II	2.8 (0.1)	839.5 (20.8)	8.5 (1.8)	44.1 (2.4)	55.9 (2.4)	36.3 (1.8)	63.6 (1.8)

Standard deviations of averages are given in parentheses. Interface parameters were evaluated by means of the PPI server.
RMSD values were calculated with respect to the complex structures at the beginning of the MD simulation (i.e., at time $t = 0$ ps).

loops belong indeed to the most flexible p53 DBD regions and they can therefore adopt a wide range of conformations to improve the p53 DBD–AZ surface matching (Klein *et al*., 2001; Pan *et al*., 2005, 2006; Ho *et al*., 2006). The p53 DBD interface in groups III and IV contains instead the L_2 and L_3 loops, that, unlike the L_1 loop, form more rigid structures tethered together by the zinc ion (Duan and Nilsson, 2006) and cannot therefore be deformed to significantly improve the surface complementarity with AZ.

The ASA behavior during the simulations is also coupled to a change in the ratio of non-polar to polar residues at the protein–protein interface. As may be seen by comparing Tables 1 and 2, in groups I and II the intermolecular interactions in aqueous environment in conjunction with the high degree of molecular surface complementarity favor the increase in hydrophobic residues at the p53 DBD binding interface, while in groups III and IV the p53 DBD non-polar interface area was found to decrease, since in these models no optimization for the shape complementary between the two molecules occurred during the simulations. AZ docking surface remained nearly unchanged with respect to the starting configurations, with the exception of models 1 and 7, where it becomes slightly more polar, and models 4, 5, and 9, where a weak increase in the hydrophobic part of the interface is observed during our MD runs. It is interesting to note that no water molecules have been found at the interface in all the models.

Finally, regarding p53 DBD–AZ hydrogen-bonding interactions, as reported in Table 2 HB values increased with respect to the starting structures in all 10 models, the maximum changes in HB corresponding, in particular, to groups I and II, in which three to eight new HBs were established between the two proteins; these additional HBs playing an important role in stabilizing the complex structures as well as contributing to p53 DBD–AZ binding specificity.

Free energy of interaction between the p53 DBD and AZ

Binding free energies for the 10 p53 DBD–AZ docking modes were evaluated applying the MM-PBSA methodology. This procedure is rapidly becoming one of the most popular computational tools for estimating binding affinities of protein–protein complexes since it produces reasonably accurate results at a moderate computational cost. Moreover the MM-PBSA binding free energy can be decomposed in terms of forcefield and solvation contributions, providing thus additional information about the forces leading to p53 DBD–AZ association.

Figure 4 shows all energy terms and the binding free energies for our docking models; the three panels, from top to bottom, showing the non-polar (E_{VdW}, $G_{non\text{-}polar,solv}$, and $G_{non-polar}=E_{VdW}+G_{non-polar,solv}$), polar ($E_{elec}$, $G_{polar,solv}$, and $G_{polar}=E_{elec}+G_{polar,solv}$), and total binding free energies, respectively.

An analysis of the temporal trend of the $G_{binding}$ has shown that all 10 complexes have reached, in the analyzed temporal window, an almost state with slight fluctuations around the average value reported in the lower panel of Figure 4.

For all 10 models the dominant contribution to $G_{binding}$ (lower panel of Figure 4) comes from the $G_{non\text{-}polar}$ component (turquoise bars in the upper panel of Figure 4), and more specifically from the E_{VdW} term (orange bars), whose absolute value constitutes on average 60% of $G_{binding}$. The most favorable values of non-polar free energies correspond, in particular, to the structures in groups I and II, due to their high degree of surface complementarity as well as to the strongly hydrophobic character of their interfaces.

In contrast to the non-polar part of $G_{binding}$, where both the Van der Waals interaction energy and the non-polar solvation term are favorable to complex formation, the two components of the polar free energy (green bars in the central panel of Figure 4) behave in opposite ways. The E_{elec} term (red bars) is favorable to the binding process, while the $G_{polar,solv}$ contribution (cyan bars) tends to favor the unbound over the bound state. The last effect is due to the large penalty for desolvation of buried polar hydrogen-bonding groups. The largest desolvation penalties are paid, in particular, by the models in groups I and II, due to their high HB values during the simulations (see Table 2).

DOI: 10.1002/jmr

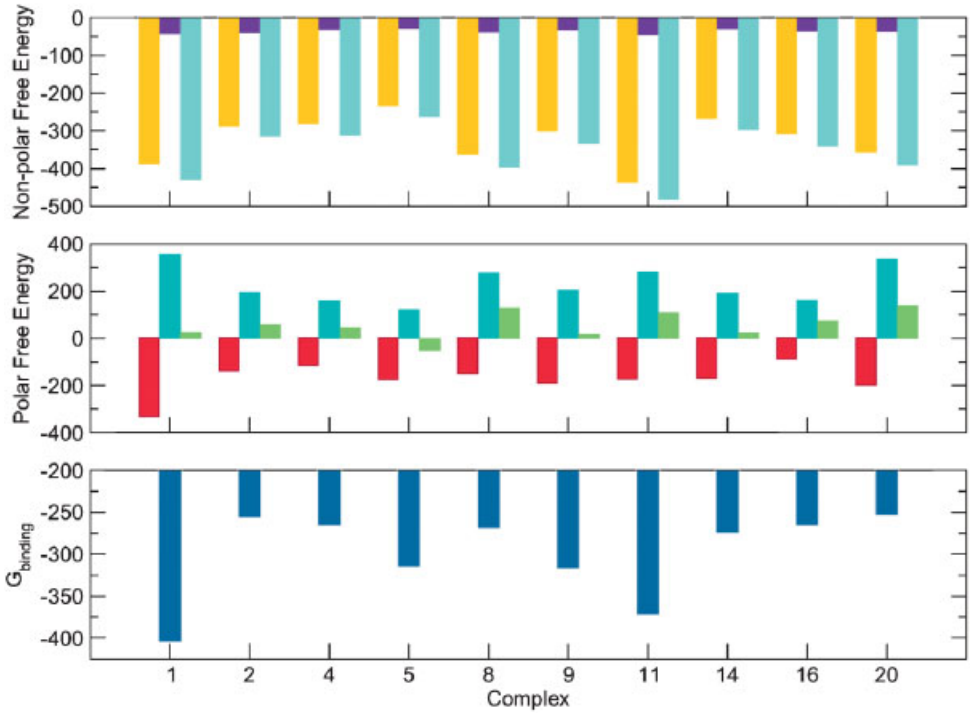

Figure 4. Panels from top to bottom show the non-polar, polar, and total binding free energies for the 10 p53 DBD–AZ binding modes. In the top panel E_{VdW} is shown in orange, $G_{non\text{-}polar,solv}$ in violet, $G_{non\text{-}polar}$ in turquoise, in the central panel E_{elec} is reported in red, $G_{polar,solv}$ in cyan and G_{polar} in green, and in the bottom panel $G_{binding}$ is shown in blue. All terms were computed over 150 MD snapshots of the complexes and are expressed in kJ mol^{-1}.

The counterplay between the two components of G_{polar} leads to an unfavorable polar contribution to binding. Actually, the desolvation effect is greater than the direct protein–protein interaction, for all models with the exception of model 4, where instead a favorable polar free energy is found. In this model in fact the p53 DBD interface has an high content in polar charged residues, yielding an highly favorable E_{elec}. On the other hand, only a few of these surface groups participate in hydrogen bonding with AZ, giving the lowest $G_{polar,solv}$ among our models. The net result is that gain of binding due to protein–protein interaction dominates the unfavorable contribution from dehydration of polar groups, thereby making the overall polar free energy favorable to protein association. Regardless if the polar free energy opposes the binding or not, its contribution to $G_{binding}$ is very small for all 10 structures, with the exception of models 5 in group I and 7 and 10 in group II. Indeed in these models the G_{polar} term represents more than 30% of the p53 DBD–AZ interaction free energy; this being due to the balance between the very high values of $G_{polar,solv}$ and quite low values of E_{elec}. The small contribution of the E_{elec} term can be attributed to both the largely hydrophobic character of the p53 DBD–AZ interface. This gives rise to higher values of Van der Waals interaction energies with respect to the Coulombic ones, and to the predominantly neutral charge of the polar residues involved in forming the numerous HB in these structures. Since the magnitude of the desolvation term is almost the double than the magnitude of the electrostatic energy, these models show the mostly unfavorable polar free energies of the 10. A similar order of magnitude in $G_{polar,solv}$ as in models 5, 7, and 10 is found also in model 1. However, in this case the higher polar binding area in conjunction with the contribution of the Coulombic energy from the charged hydrogen-bonding residues Glu 221, Glu 224, and Asp 228 on the p53 DBD s_7–s_8 loop yield a larger value of E_{elec}. This highly favorable Coulombic interaction energy almost compensates the strongly unfavorable $G_{polar,solv}$ contribution, giving thus a very small positive value of G_{polar} for model 1.

Finally, regarding the overall p53 DBD–AZ binding affinities, as may be seen in the bottom panel of Figure 4, the ranking order of the 10 models based on their relative free energies differs from the starting docking score (see Table 1), highlighting thus the important role of both protein flexibility and solvation effects in determining protein–protein recognition specificity.

Nonetheless, the model having the most favorable $G_{binding}$ value corresponds to the first-ranked solution also according to the docking score function and it is characterized by a p53 DBD–AZ interaction free energy of -403.5 kJ mol^{-1}, about 32.5 kJ mol^{-1} more negative than the second best prediction (corresponding to model 7).

Figure 5A shows the superimposition between the 3D structures of model 1 before (depicted in teal) and after (depicted in red) the MD simulation. As may be seen by comparing the simulated structure with the initial docking configuration, during our MD run the p53 DBD interfacial region for AZ undergoes significant conformational changes, the largest structural modifications being found in particular in the flexible L_1 and s_7–s_8 loops, leading to a tighter p53 DBD–AZ packing with respect to the starting model. As a consequence of the structural rearrangement in the docking interface, very favorable Van der Waals contacts (see orange bars in the top panel of Figure 4), mainly

DOI: 10.1002/jmr

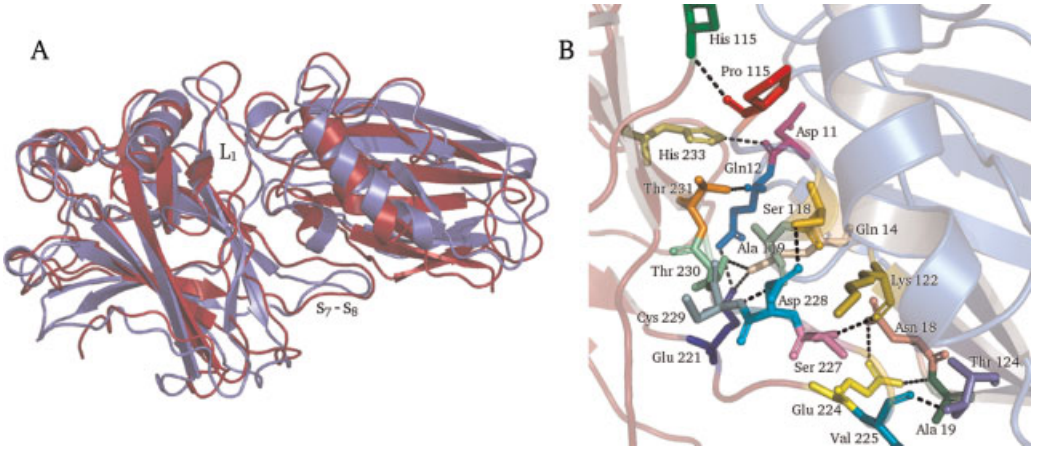

Figure 5. A. Superimposition of the p53 DBD–AZ conformation in model 1 before (teal) and after (red) the MD run. B. HB network in the simulated structure of model 1. p53 and AZ are depicted in red and blue ribbon representations, respectively. Intermolecular HBs are drawn as dashed lines. This figure is available in colour online at www.interscience.wiley.com/journal/jmr

involving AZ residues in the HP and p53 DBD residues on L_1, and HBs (see Figure 5B), mainly involving p53 DBD residues on s_7–s_8, are established between the two proteins; these extensive p53 DBD–AZ interactions resulting in a good degree of both geometric surface matching (see ASA of model 1 in Table 2) and electrostatic complementarity (see Figure 6) between the two molecules.

The reliability of the proposed model was further evaluated by checking its consistency against currently available experimental mutagenesis data (Yamada *et al*., 2002). To investigate the effects of mutations at the protein–protein interface, we calculated the difference in binding free energies between WT and mutant (AZ M44KM64E) forms of model 1. The results of the free energy calculation for the mutant complex are presented in Table 3, where also the corresponding quantities for WT model are reported for comparison.

A significant loss of about 75 kJ mol^{-1} is found in the interaction free energy of the mutant complex with respect to WT, consistent with the experimental finding that AZ residues Met 44 and Met 64 are critical for binding to p53. Almost all the free energy difference between mutated and WT model 1 arises, in particular, from $G_{\text{non-polar}}$, since substitution of two non-polar residues with polar charges ones strongly weakens hydrophobic interactions with the non-polar groups in the L_1 loop of the p53 DBD. As a consequence of the loss in protein–protein Van der Waals contacts, a poorer degree of geometric surface matching is observed for the mutant model with respect to WT, the average ASA of the p53 DBD–AZ M44KM64E complex during the simulation resulting 840 Å^2, about 140 Å^2 lower than WT (see Table 2). Regarding the polar components of G_{binding}, even if the two complexes possess similar total

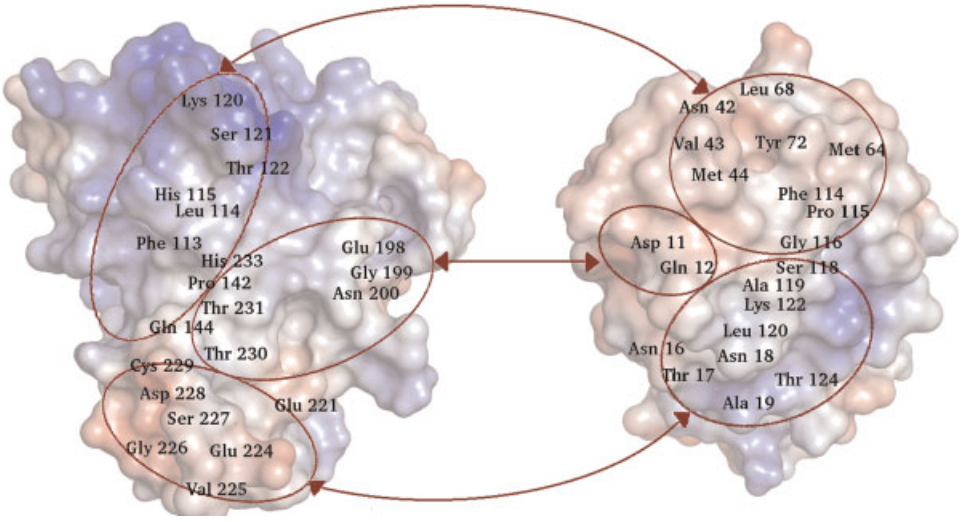

Figure 6. Electrostatic surface potential of the p53 DBD (on the left) and AZ (on the right) in model 1, as calculated by the APBS program. Each molecule is viewed from the top of its docking interface. The p53 DBD L_1 loop and s_3 strand complement the AZ β_3–β_4, β_4–β_5, and β_7–β_8 connections, the p53 DBD s_5–s_6 loop and s_3 strand bind to the AZ β_2 strand and the p53 DBD s_7–s_8 loop associates with AZ residues on the β_1–β_2 loop and on β_8. Positive potentials are shown in blue, negative in red. This figure is available in colour online at www.interscience.wiley.com/journal/jmr

DOI: 10.1002/jmr

Table 3. Free energy of interaction for the M44KM64E mutant and WT p53 DBD–AZ complex

	E_{elec}	E_{VdW}	$G_{non\text{-}polar,solv}$	$G_{polar,solv}$	G_{polar}	$G_{non\text{-}polar}$	$G_{binding}$
Mutant	−202.1	−317.4	−35.3	226.3	24.2	−352.6	−328.4
WT	−332.5	−386.9	−41.2	357.1	24.6	−428.1	−403.5

All terms are expressed in kJ mol^{-1}.

G_{polar} values, in the mutant model both the E_{elec} and $G_{polar,solv}$ terms are significantly lower in magnitude with respect to WT. The 130 kJ mol^{-1} decrease in protein–protein electrostatic energy for the mutant complex, in particular, may be ascribed to loss in hydrogen-bonding interactions due to removal upon mutation of four intermolecular HB, involving AZ residues on the β_1–β_2 and β_7–β_8 loops and p53 DBD polar charged residues Glu 221, Glu 224, and Asp 228 on the s_7–s_8 loop. Therefore replacement of AZ residues Met 44 and Met 64 does affect its interaction with both the contacting L_1 loop and the non-contacting s_7–s_8 loop. Since some motional correlation between L_1 and s_7–s_8 was previously observed (Pan *et al*., 2005, 2006), it is likely that introduction of a mutation destabilizing AZ binding to L_1 also abolishes some protein–protein tight packing contacts involving s_7–s_8, yielding thus lower p53 DBD–AZ geometric and electrostatic complementarity with respect to WT model.

It is worth noting that the L_1 and s_7–s_8 loops are the most unstable regions in the p53 DBD, due to their very loose packing against each other or against the β-sheet core (see for instance Figure 5A), resulting in very high mobility (Klein *et al*., 2001; Pan *et al*., 2005, 2006; Ho *et al*., 2006). In our best docking model AZ binds to both these p53 DBD motifs and this result confirms that conformational flexibility plays a key role in determining macromolecular recognition specificity, allowing for high efficiency and rapid turn-over of protein–protein interactions (Lu *et al*., 2007). Furthermore, the observed AZ binding to these mobile loops makes it possible to propose a molecular mechanism for the increase in p53 stability upon complex formation with AZ. More specifically, we hypothesize that the p53-stabilizing effect of AZ could arise from the strong Van der Waals and hydrogen-bonding interactions established between the most flexible residue regions of the p53 DBD L_1 (residues 113–115) and s_7–s_8 (residues 221 and 224–229) loops and AZ residues in the HP and on the β_1–β_2 and β_7–β_8 connections (see Figure 5B); these extensive protein–protein interactions reducing mobility and increasing stability for the p53 DBD peripheral loops. Such a possible structure–function relationship for the investigated complex is particularly interesting and deserves further study in view of potential therapeutic applications based on p53–AZ interaction.

A variety of mutations can be proposed for a validation of the found best complex model. Single residue mutations of AZ or p53 residues involved at the interface could be performed. For instance, it can be investigated if the replacement of charged residues with a non-polar residue modifies the affinity of the two protein partners in the complex. In particular, we propose to mutate residues such as Lys122 or Asp11 of AZ, forming HB with p53 at the interface.

CONCLUSIONS

In this work rigid-body protein docking combined with MD simulations and free energy calculations allowed mapping the protein–protein interface within the p53 DBD–AZ complex, complementing previous experimental studies about the interaction between these two molecules. A three-dimensional model for the complex was singled out among a large number of predicted structures and validated by using a computational mutagenesis strategy. In the proposed model the binding interface involves many close contacts between the highly flexible L_1 and s_7–s_8 loops of the p53 DBD and residues in the HP of AZ. Since the L_1 and s_7–s_8 loops are the most unstable regions in the p53 DBD, we suggest that AZ binding to these peripheral motifs may enhance their stability by restraining their flexibility, providing thus a possible structural basis for understanding the p53-stabilizing action of AZ. The predicted p53 DBD–AZ binding mode thus supports the idea that the p53 DBD flexible motifs might be targets for p53-stabilizing molecules. Information about AZ interaction mode with these regions from the present work can provide a useful starting point to design new drug compounds mimicking the p53 DBD–AZ interface for anticancer therapeutics. The results of our study finally point out that protein docking procedures integrated with free energy simulations and computational mutagenesis are powerful tools for modeling protein complexes interactions.

Acknowledgments

This work has been partially supported by an Innesco-CNISM project 2005 and two PRIN-MIUR 2006 projects (numbers 2006028219 and 2006027587).

REFERENCES

Apiyo D, Wittung-Stafshede P. 2005. Unique complex between bacterial azurin and tumor-suppressor protein p53. *Biochem. Biophys. Res. Commun.* **332**: 965–968.

Arcangeli C, Bizzarri AR, Cannistraro S. 1999. Long-term molecular dynamics simulation of copper azurin: structure, dynamics and functionality. *Biophys. Chem.* **78**: 247–257.

Baker NA, Sept D, Joseph S, Holst MJ, McCammon JA. 2001. Electrostatics of nanosystems: application to microtubules and the ribosome. *Proc. Natl. Acad. Sci. USA* **98**: 10037–10041.

Bell S, Hansen S, Buchner J. 2002. Refolding e structural characterization of the human p53 tumor suppressor protein. *Biophys. Chem.* **96**: 243–257.

Berendsen HJC, Postma JPM, van Gunsteren WF, Hermans J. 1969. Interaction models for water in relation to protein hydration. *Nature* **224**: 175–177.

Bizzarri AR. 2006. Topological and dynamical properties of Azurin anchored to a gold substrate as investigated by molecular dynamics simulation. *Biophys. Chem.* **122**: 206–214.

Bizzarri AR, Brunori E, Bonanni B, Cannistraro S. 2007. Docking and molecular dynamics simulation of the azurin-cytochrome c551 electron transfer complex. *J. Mol. Recogn.* **20**: 122–131.

Bonander N, Leckner J, Guo H, Karlsson BG, Sjölin L. 2000. Crystal structure of the disulfide bond-deficient azurin mutant C3A/C26A. How important is the S-S bond for folding and stability? *Eur. J. Biochem.* **267**: 4511–4519.

Bonanni B, Kamruzzahan ASM, Bizzarri AR, Rankl C, Gruber HJ, Hinterdorfer P, Cannistraro S. 2005. Single molecule recognition between cytochrome C 551 and gold-immobilized azurin by force spectroscopy. *Biophys. J.* **89**: 2783–2791.

Calimet N, Simonson T. 2006. Cys_xHis_y-Zn^{2+} interactions: possibilities and limitations of a simple pairwise force field. *J. Mol. Graph. Model.* **24**: 404–411.

Cascella M, Magistrato A, Tavernelli I, Carloni P, Rothlisberger U. 2006. Role of protein frame and solvent for the redox properties of azurin from Pseudomonas aeruginosa. *Proc. Natl. Acad. Sci. USA* **103**: 19641–19646.

Chen R, Weng Z. 2002. Docking unbound proteins using shape complementarity, desolvation, and electrostatics. *Proteins: Struct. Funct. Genet.* **47**: 281–294.

Chen R, Weng Z. 2003. A novel shape complementarity scoring function for protein-protein docking. *Proteins: Struct. Funct. Genet.* **51**: 397–408.

Cho Y, Gorina S, Jeffrey PD, Pavletich NP. 1994. Crystal structure of a p53 tumor suppressor-DNA complex: understanding tumorigenic mutations. *Science* **265**: 346–355.

Chong LT, Duan Y, Wang L, Massova I, Kollman PA. 1999. Molecular dynamics and free-energy calculations applied to affinity maturation in antibody 48G7. *Proc. Natl. Acad. Sci. USA* **96**: 14330–14335.

Clore GM, Omichinski JG, Sakaguchi K, Zambrano N, Sakamoto H, Appella E, Gronenborn AM. 1994. High-resolution structure of the oligomerization domain of p53 by multidimensional NMR. *Science* **265**: 386–391.

Comeau SR, Gatchell DW, Vajda S, Camacho CJ. 2004. ClusPro: a fully automated algorithm for protein– protein docking. *Nucleic Acids Res.* **32**: 96–99.

Dawson R, Muller L, Dehner A, Klein C, Kessler H, Buchner J. 2003. The N-terminal domain of p53 is natively unfolded. *J. Mol. Biol.* **332**: 1131–1141.

De Rienzo F, Gabdoulline RR, Menziani MC, Wade RC. 2000. Blue copper proteins: a comparative analysis of their molecular interaction properties. *Protein Sci.* **9**: 1439–1454.

Duan J, Nilsson L. 2006. Effect of Zn^{2+} on DNA recognition and stability of the p53 DNA-binding domain. *Biochemistry* **45**: 7483–7492.

Ganoth A, Friedman R, Nachliel E, Gutman M. 2006. A molecular dynamics study and free energy analysis of complexes between the Mlc1p protein and two IQ motif peptides. *Biophys. J.* **91**: 2436–2450.

Guex N, Peitsch MC. 1997. SWISS-MODEL and the Swiss-PdbViewer: an environment for comparative protein modeling. *Electrophoresis* **18**: 2714–2723.

Halperin I, Ma B, Wolfson H, Nussinov R. 2002. Principles of docking: an overview of search algorithms and a guide to scoring functions. *Proteins: Struct. Funct. Genet.* **47**: 409–443.

Hess B, Bekker H, Berendsen HJC, Fraaije JGEM. 1997. LINCS: a linear constraint solver for molecular simulations. *J. Comp. Chem.* **18**: 1463–1472.

Ho WC, Luo C, Zhao K, Chai X, Fitzgerald MX, Marmorstein R. 2006. High-resolution structure of the p53 core domain: implications for binding small-molecule stabilizing compounds. *Acta Cryst.* **D62**: 1484–1493.

Humphrey WF, Dalke A, Schulten K. 1996. VMD—visual molecular dynamics. *J. Mol. Graph.* **14**: 33–38.

Jeffrey PD, Gorina S, Pavletich NP. 1995. Crystal structure of the tetramerization domain of the p53 tumor suppressor at 1.7 angstroms. *Science* **267**: 1498–1502.

Joerger AC, Ang HC, Fersht AR. 2006. Structural basis for understanding oncogenic p53 mutations and designing rescue drugs. *Proc. Natl. Acad. Sci. USA* **103**: 15056–15061.

Jones S, Thornton JM. 1996. Principles of protein-protein interactions derived from structural studies. *Proc. Natl. Acad. Sci. USA* **93**: 13–20.

Klein C, Planker E, Diercks T, Kessler H, Künkele KP, Lang K, Hansen S, Schwaiger M. 2001. NMR spectroscopy reveals the solution dimerization interface of p53 core domains bound to their consensus DNA. *J. Biol. Chem.* **276**: 49020–49027.

Liu J, Pan Y, Ma B, Nussinov R. 2006. 'Similarity trap' in protein-protein interactions could be carcinogenic: simulations of p53 core domain complexed with 53BP1 and BRCA1 BRCT domains. *Structures* **14**: 1811–1821.

Lu Q, Lu HP, Wang J. 2007. Exploring the mechanism of flexible biomolecular recognition with single molecule dynamics. *Phys. Rev. Lett.* **98**: 128105-1–128105-4.

Masatoshi G, Yamada T, Kimbara K, Horner J, Newcomb M, Das Gupta TK, Chakrabarty AM. 2003. Induction of apoptosis in macrophages by Pseudomonas aeruginosa azurin: tumor-suppressor protein p53 and reactive oxygen species, but not redox activity, as critical elements in cytotoxicity. *Mol. Microbiol.* **47**: 549–559.

Massova I, Kollman PA. 1999. Computational alanine scanning to probe protein-protein interactions: a novel approach to evaluate binding free energies. *J. Am. Chem. Soc.* **121**: 8133–8143.

Maynard AT, Covell DG. 2001. Reactivity of zinc finger cores: analysis of protein packing and electrostatic screening. *J. Am. Chem. Soc.* **123**: 1047–1058.

McDonald IK, Thornton JM. 1994. Satisfying hydrogen-bonding potential in proteins. *J. Mol. Biol.* **238**: 777–793.

Nar H, Messerschmidt A, Huber R, van de Kamp M, Canters GW. 1991. Crystal structure analysis of oxidized Pseudomonas aeruginosa azurin at pH 5.5 and pH 9.0. A pH-induced conformational transition involves a peptide bond flip. *J. Mol. Biol.* **221**: 765–772.

Nooren IMA, Thornton JM. 2003. Structural characterization and functional significance of transient protein-protein interactions. *J. Mol. Biol.* **325**: 991–1018.

Pan Y, Ma B, Venkataraghavan RB, Levine AJC, Nussinov R. 2005. In the quest for stable rescuing mutants of p53: computational mutagenesis of flexible loop L1. *Biochemistry* **44**: 1423–1432.

Pan Y, Ma B, Levine AJ, Nussinov R. 2006. Comparison of the human and worm p53 structures suggests a way for enhancing stability. *Biochemistry* **45**: 3925–3933.

Pérez Cañadillas JM, Tidow H, Freund SMV, Rutherford TJ, Ang HC, Fersht AR. 2006. Solution structure of p53 core domain: structural basis for its instability. *Proc. Natl. Acad. Sci. USA* **103**: 2109–2114.

Punji V, Das Gupta TK, Chakrabarty AM. 2003. Bacterial cupredoxin azurin and its interactions with the tumor suppressor protein p53. *Biochem. Biophys. Res. Commun.* **312**: 109–114.

Punj V, Bhattacharyya S, Saint-Dic D, Vasu C, Cunningham EA, Graves J, Yamada T, Constantinou AI, Christov K, White B, Li G, Majumdar D, Chakrabarty AM, Das Gupta TK. 2004. Bacterial cupredoxin azurin as an inducer of apoptosis and regression in human breast cancer. *Oncogene* **23**: 2367–2378.

DOI: 10.1002/jmr

Sheinerman FB, Norel R, Honig B. 2000. Electrostatic aspects of protein-protein interactions. *Curr. Opin. Struct. Biol.* **10**: 153–159.

Srinivasan J, Cheatham TE, Cieplak P, Kollman PA, Case DA. 1998. Continuum solvent studies of the stability of DNA, RNA, and phosphoramidate—DNA helices. *J. Am. Chem. Soc.* **120**: 9401–9409.

Swart M. 2002. *Density functional theory applied to copper proteins*. PhD Thesis; Groningen, Rijksuniversiteit Groningen.

Vajda S, Camacho CJ. 2004. Protein–protein docking: is the glass half-full or half-empty? *Trends Biotechnol.* **22**: 110–116.

van der Spoel D, van Buuren AR, Apol E, Meulenhoff PJ, Tieleman DP, Sijbers ALTM, Hess B, Feenstra KA, Lindahl E, van Drunen R, Berendsen HJC. 2001. *GROMACS User Manual*. University of Groningen, Groningen: The Netherlands; Version 3.2.

Veprintsev DB, Freund SMV, Andreeva A, Rutledge SE, Tidow H, Pérez Cañadillas JM, Blair CM, Fersht AR. 2006. Core domain interactions in full-length p53 in solution. *Proc. Natl. Acad. Sci. USA* **103**: 2115–2119.

Vogelstein B, Lane DP, Levine AJ. 2000. Surfing the p53 network. *Nature* **408**: 307–310.

Webb MA, Loppnow GR. 1999. A structural basis for long-range coupling in azurins from resonance Raman spectroscopy. *J. Phys. Chem. A* **103**: 6283–6287.

Weinberg RL, Freund SMV, Veprintsev DB, Bycroft M, Fersht AR. 2004. Regulation of DNA binding of p53 by its C-terminal domain. *J. Mol. Biol.* **342**: 801–811.

Wong KB, DeDecker BS, Freund SMV, Proctor MR, Bycroft M, Fersht AR. 1999. Hot-spot mutants of p53 core domain evince characteristic local structural changes. *Proc. Natl. Acad. Sci. USA* **96**: 8438–8442.

Wu Y, Cao Z, Yi H, Jiang D, Mao X, Liu H, Li W. 2004. Simulation of the interaction between ScyTx and small conductance calcium-activated potassium channel by docking and MM-PBSA. *Biophys. J.* **87**: 105–112.

Yamada T, Goto M, Punj V, Zaborina O, Chen ML, Kimbara K, Majumdar D, Cunningham E, Das Gupta TK, Chakrabarty AM. 2002. Bacterial redox protein azurin, tumor suppressor protein p53, and regression of cancer. *Proc. Natl. Acad. Sci. USA* **99**: 14098–14103.

Yamada T, Hiraoka Y, Ikehata M, Kimbara K, Avner BS, Das Gupta TK, Chakrabarty AM. 2004. Apoptosis or growth arrest: modulation of tumor suppressor p53's specificity by bacterial redox protein azurin. *Proc. Natl. Acad. Sci. USA* **101**: 4770–4775.

DOI: 10.1002/jmr